B-spline *R*-matrix-with-pseudostates calculations for electron collisions with aluminum

Viktor Gedeon, Sergej Gedeon, Vladimir Lazur, and Elizabeth Nagy
Department of Theoretical Physics, Uzhgorod State University, Uzhgorod, 88000, Ukraine

Oleg Zatsarinny* and Klaus Bartschat†
Department of Physics and Astronomy, Drake University, Des Moines, Iowa, 50311, USA
(Received 8 September 2015; published 2 November 2015)

A systematic study of angle-integrated cross sections for electron scattering from neutral aluminum is presented. The calculations cover elastic scattering, excitation of the 14 states $(3s^2np)\,^2P^o$ $(n = 3,4,5,6)$, $(3s^2ns)\,^2S$ $(n = 4,5,6)$, $(3s^2nd)\,^2D$ $(n = 3,4)$, $(3s3p^2)\,^{4,2}P$, ^2D, ^2S, and $(3s^24f)\,^2F^o$, as well as electron impact ionization. The sensitivity of the results to changes in the theoretical model is checked by comparing predictions from a variety of approximations, including a large-scale model with over 500 continuum pseudostates. The current results are believed to be accurate at the few-percent level and should represent a sufficiently extensive set of electron collision data for most modeling applications involving neutral aluminum.

DOI: 10.1103/PhysRevA.92.052701 PACS number(s): 34.80.Bm, 34.80.Dp

I. INTRODUCTION

Collisions of electrons with atomic aluminum and its compounds find applications in different fields of research and industry. For example, electrons impinging on metals like aluminum serve as important tools in electron microscopy, surface electron spectroscopy, microlithography, and electron probe microanalysis, to name just a few. Their Monte Carlo simulations require reliable cross sections [1]. Furthermore, electron impact ionization studies of the metal oxide molecules of Al are important in materials research. Aluminum is also found as an impurity in the plasma edge of nuclear fusion reactors [2], such as the Madison Symmetric Torus [3] with Al walls. Plasma-wall interactions in fusion devices liberate impurities, and modeling possible impurity transport requires accurate ionization and recombination rate coefficients [4].

Until now collisions of electrons with aluminum atoms have not been investigated thoroughly, due to both experimental and theoretical challenges. We know only that cross-section measurements have been reported for the $3s^23p$-$3s^24s$ and $3s^23p$-$3s^23d$ optically allowed transitions [5] and for the ionization process [6]. Due to the lack of experimental data, researchers in plasma modeling currently have to rely entirely on theoretical predictions. For this reason, it is important to estimate the accuracy of the available theoretical data. Theoretical studies of electron scattering on Al, however, are very scarce as well. Many years ago, Ryabikh and Fabricant [7] carried out a calculation for low-energy elastic cross sections in a two-state close-coupling (CC-2) approximation, the results of which are still being used today. Ionization of Al by electron impact has been studied in some more detail. Kim and Stone [8] predicted direct ionization cross sections for Al, Ga, and In based on the semiempirical binary-encounter-Bethe (BEB) model. They also found substantial contributions from the excitation-autoionization process for these atoms. More recently, ionization of aluminum was thoroughly treated by Loch *et al.* [9] within advanced *R*-matrix with pseudostates (RMPS) and time-dependent close-coupling (TDCC) methods. However, detailed investigations were reported neither for elastic scattering nor for state-to-state excitation processes.

The objective of the current work, therefore, was to carry out a comprehensive study of electron collisions with neutral aluminum, including a thorough sensitivity analysis of the theoretical predictions on the details of the computational model. Such an analysis is of critical importance in light of the growing demand for theorists to estimate the uncertainty of their results in some form [10,11]. As a by-product of this work, an extensive set of electron collision data for neutral aluminum, including elastic scattering, momentum transfer, excitation, and ionization from the ground state has been generated and will be made available to the public.

The calculations reported below were carried out with our *B*-spline *R*-matrix (close-coupling) code BSR [12]. Calculations for many neutral target atoms, but especially for open-shell systems such as Al, where intrashell correlations (here between the $3s$ and the $3p$ subshells) are important, are highly challenging due to the difficulties faced already in achieving a good description of the target structure. The distinct feature of the BSR approach and the corresponding general computer code is its ability to employ term-dependent nonorthogonal orbital sets in the description of the target states. This allows us to optimize individual atomic wave functions independently and thereby to generate a more accurate description of the target states than what is usually possible when orthogonality restrictions are imposed. Over the past decade, the BSR code (along with its full-relativistic extension, DBSR [13]) has been successfully applied to a number of targets [14], and in many cases the cross sections are believed to be more accurate than what was obtained using the standard *R*-matrix technique. Note that the BSR suite of programs forms a general code for many-electron targets. Its advantages are particularly seen in cases of electron scattering from systems with complex configurational structure, including multiple open shells [14]. Its application in the large-scale nonperturbative RMPS mode usually requires massively parallel computers.

This manuscript is organized as follows: After discussing the description of the target structure, we summarize the most important aspects of the collision calculations. This is followed

*oleg.zatsarinny@drake.edu
†klaus.bartschat@drake.edu

by a presentation of the cross sections for the most important transitions, starting with elastic electron scattering from Al in its ground state, followed by state-to-state transitions between discrete states, and finally ionization. Comparison of results obtained in different models provides an estimate regarding the likely accuracy of the present data set.

II. COMPUTATIONAL DETAILS

A. Structure calculations

The target states of aluminum in the present calculations were generated by combining the multiconfiguration Hartree-Fock (MCHF) and the B-spline box-based close-coupling methods [15]. The aluminum atom was treated effectively as a three-active-electron system above the frozen $1s^2 2s^2 2p^6$ core. Since relativistic effects are relatively small in aluminum, we used the nonrelativistic LS-coupling approximation. The ground state of Al has the principal configuration $3s^2 3p$, and many excited states have the apparently simple structure $3s^2 nl$. The $3s^2 nd$ Rydberg series, however, is strongly perturbed by the $3s$-excited state $(3s3p^2)\,^2D$. This is a classical example of an extremely strong interaction between a perturber and a Rydberg series, when the perturber loses its identity and is smeared out over the entire series [16]. Despite their one-electron character, the $3s^2 nl$ states are also correlated states due to significant admixtures from $3p^2 nl$ configurations and the strong dipole promotion of the $3s$ electron to the $3p$ subshell.

To address all these effects, we chose the structure of the multichannel target expansion as

$$\begin{aligned}\Phi(3s^2 nl, LS) = &\sum_{nl}\{\phi(3s^2)P(nl)\}^{LS} \\ &+ \sum_{nl,L'S'}\{\phi(3s3p, L'S')P(nl)\}^{LS} \\ &+ \sum_{nl,L'S'}\{\phi(3p^2, L'S')P(nl)\}^{LS} \\ &+ a\varphi(3s^2 3p)^2 P^o + b\varphi(3s3p^2)^{LS}. \quad (1)\end{aligned}$$

Here $P(nl)$ denotes the orbital of the outer valence electron, while the ϕ and φ functions represent the configuration interaction (CI) expansions of the corresponding ionic and specific atomic states, respectively. These expansions were generated in separate MCHF calculations for each state using the MCHF program [17]. They include all single and double excitations from the $3s$ and $3p$ orbitals to the $4l$ ($l = 0 - 3$) correlated orbitals. These wave functions ensure the proper inclusion of important short-range correlation effects.

Expansion (1) may be considered as a model for the entire $3s^2 nl$ Rydberg series of the aluminum spectrum, including the continuum pseudostates lying above the ionization limit. The expansion also provides a good approximation for the ground-state configuration $3s^2 3p$, as well as for the core-excited states $(3s3p^2)^{LS}$. Alternatively, we can choose to employ separate CI expansions for these states by directly including relaxation effects via state-specific one-electron orbitals. The latter way is preferable and allows us to control the accuracy of these highly correlated states by using extensive CI expansions. This is particularly important in the case of a strong interaction of a perturber with a Rydberg series, where small changes in the perturber expansion may lead to radical changes in its position relative to the other states.

TABLE I. Binding energies (in eV) for the spectroscopic target states included in our CC expansion.

State	Term	NIST [19]	Present	Diff.
$3s^2 3p$	$^2P^o$	−5.976	−5.946	0.030
$3s^2 4s$	^2S	−2.843	−2.808	0.035
$3s3p^2$	^4P	−2.378	−2.384	−0.006
$3s^2 3d$	^2D	−1.964	−1.950	0.014
$3s^2 4p$	$^2P^o$	−1.899	−1.890	0.009
$3s^2 5s$	^2S	−1.313	−1.302	0.011
$3s^2 4d$	^2D	−1.159	−1.158	0.001
$3s^2 5p$	$^2P^o$	−0.992	−0.988	0.004
$3s^2 4f$	$^2F^o$	−0.863	−0.863	0.000
$3s^2 6s$	^2S	−0.761	−0.751	0.010
$3s^2 5d$	^2D	−0.749	−0.747	0.002
$3s^2 6p$	$^2P^o$	−0.613	−0.590	0.023
$3s3p^2$	^2S	0.431	0.423	−0.008
$3s3p^2$	^2P	1.044	1.086	0.042

The unknown functions $P(nl)$ for the outer valence electron were expanded in a B-spline basis, and the corresponding equations were solved subject to the condition that the wave functions vanish at the boundary. The B-spline coefficients for the valence orbitals $P(nl)$, along with the coefficients a and b (when needed for a particular LS symmetry), were obtained by diagonalizing the N-electron atomic Hamiltonian. The number of spectroscopic bound states that can be generated in the above scheme depends on the B-spline box radius. In most of the present calculations, the latter was set to $50a_0$, where $a_0 = 0.529 \times 10^{-10}$ m is the Bohr radius. This allowed us to obtain good descriptions of the aluminum states with principal quantum number for the valence electron up to $n = 6$. The remaining eight negative-energy pseudostates in this box-based pseudostates approach (see [18] for a general discussion of the underlying ideas) are an approximate way to account for the infinite number of Rydberg states.

The expansion (1) is also able to generate continuum pseudostates lying above the ionization threshold. The density and number of these states mostly depend on the box radius and to a lesser extent on other B-spline parameters, such as their order or distribution on the grid. The above approach is both a straightforward and general way to obtain the continuum pseudospectrum. It provides excellent flexibility regarding its quality by allowing us to choose different box radii or changing the density of the B-spline basis. However, since these calculations generate different nonorthogonal sets of orbitals for each atomic state, their subsequent use requires the ability to treat the nonorthogonal orbitals in a general way. This possibility is provided by the BSR code.

Table I compares the calculated spectrum of neutral aluminum with the experimental values [19] for various LS multiplets included in the scattering calculations (see below). The overall agreement between experiment and theory is very satisfactory, with the deviation in the energy splitting being less than 42 meV for all states, including also the important

core-excited $3s3p^2$ states. The $3s3p^2\ ^2D$ state, in particular, deserves special consideration. Due to its strong interaction with the $3s^2nd$ Rydberg series, the $3s3p^2\ ^2D$ state completely loses its identity and spreads out over the entire series. For example, its admixtures to the first few levels are 21%, 23%, 14%, and 10% for the $3d$, $4d$, $5d$, and $6d$ states, respectively. Thereby, in accordance with the analysis [16], none of the states of the ^2D series can unambiguously be identified with the $3s3p^2\ ^2D$ state. This conclusion is also supported by determining the number of nodes in the corresponding nd orbitals. In this respect, the labeling "$3d$, nd, $4d$, $5d$, $6d$" of the respective states in the NIST compilation [19] does not seem to be a suitable assignment. We suggest to replace the perturber label "nd" by "$4d$" and then reduce the principal quantum numbers for the subsequent levels of this series by one.

TABLE II. Comparison of oscillator strengths in Al. The quantities in square brackets represent the power of 10.

Transition	f_L	% diff.[a]	NIST [19]	% diff.[b]
$3p$-$4s$	1.16[−1]	2.8	1.16[−1]	0.0
$3p$-$3d$	1.74[−1]	1.6	1.70[−1]	2.3
$3p$-$5s$	1.44[−2]	3.8	1.50[−2]	4.1
$3p$-$4d$	4.62[−2]	1.4	4.90[−2]	5.9
$3p$-$6s$	5.14[−3]	4.1	4.85[−3]	5.8
$3p$-$5d$	1.26[−1]	1.7	1.28[−1]	1.6
$4s$-$4p$	1.22	1.2	1.24	1.6
$4s$-$5p$	1.95[−2]	4.1	2.03[−2]	4.0
$4s$-$6p$	3.34[−3]	7.2	3.19[−3]	4.6
$3d$-$4p$	2.37[−2]	4.8	2.27[−2]	4.3
$3d$-$5p$	1.05[−3]	4.4	9.94E-4	5.5
$3d$-$4f$	4.01[−1]	0.1	3.70[−1]	8.0
$4p$-$5s$	2.56[−1]	1.1	2.01[−1]	24.1
$4p$-$4d$	7.80[−1]	1.6	8.28[−1]	6.0
$4p$-$6s$	2.40[−2]	1.7	2.36[−2]	1.7
$4p$-$5d$	4.60[−3]	7.3	4.78[−3]	3.8
$5s$-$5p$	1.71	0.6	1.74	1.7
$5s$-$6p$	4.91[−2]	1.9	4.65[−2]	5.4
$4d$-$5p$	2.09[−1]	3.0	1.94[−1]	7.4
$4d$-$4f$	7.93[−1]	0.1	7.90[−1]	0.4
$4d$-$6p$	4.77[−3]	7.8	5.35[−3]	11.5
$5p$-$6s$	4.01[−1]	0.6	3.94[−1]	1.8
$5p$-$5d$	1.21	1.4	1.25	3.3
$4f$-$5d$	1.60[−1]	0.4	1.63[−1]	1.9
$6s$-$6p$	2.24	0.4	2.18	2.7
$5d$-$6p$	3.85[−1]	1.8	3.53[−1]	8.7

[a]Percentage difference between the present L and V values.
[b]Percentage difference between the present and NIST values.

The quality of our target description can be further assessed by comparing the results for the oscillator strengths of various transitions with experimental data and other theoretical predictions. Accurate oscillator strengths are very important to obtain reliable absolute values for the excitation cross sections, especially for optically allowed transitions at high incident electron energies. A comparison of our oscillator strengths is given in Table II with the recommended data from the NIST compilation [19]. The f values for the fine-structure transitions were converted to the multiplet LS values. We see good agreement with experiment for all these transitions, with an average percentage difference of about 5%.

Table II also contains the ratio of theoretical oscillator strengths obtained in the length and velocity forms of the electric dipole operator. This ratio can, to some extent, also be considered a quality indicator for the calculated f values. For most transitions, the length (f_L) and velocity (f_V) values agree within a few percent. Notable exceptions are the $(3s^24p)^2P - (3s^25s)^2S$ and $(3s^24d)^2D - (3s^26p)^2P$ transitions, where the deviations in the two gauges exceed 10%.

B. Collision calculations

In order to check the sensitivity of the results to the size of the close-coupling expansion we carried out a set of calculations with different numbers of target states. We began with the computationally simplest model including the lowest ten spectroscopic states of aluminum of primary interest. This model will be denoted as BSR-10. Next, we included all states up to the $(3s3p^2)^2P$ autoionizing state to check the influence of the important inner-subshell $3s$-$3p$ excitation (BSR-32). As our principal model, we then carried out 81-state calculations (BSR-81). This model additionally included continuum pseudostates up to 10 eV above the ionization threshold. It is generally considered sufficient to account for the main influence of coupling to the target continuum. We also carried out a set of two-state calculations, which are close to the distorted-wave approximation. All these calculations could still be performed on modern one-processor computers.

The *ab initio* description of the ionization process, on the other hand, requires the consideration of many more continuum pseudostates. To cover the target continuum to a larger extent, we reduced the box radius to $30a_0$ and set up the BSR-587 model with 23 states representing the bound spectrum and the remaining 564 the target continuum corresponding to ionization of the $3p$ and $3s$ subshells. We included all doublet and quartet target states of principal configurations $3s^2nl$ and $3s3p(^{1,3}P)nl$ with orbital angular momentum $l = 0-3$ for the outer electron and total orbital angular momenta $L = 0-4$. The continuum pseudostates now covered the energy region up to 60 eV above the ionization limit. This model requires the parallelized version of our code to run on supercomputers with hundreds of processors.

The close-coupling equations were solved by means of the R-matrix method, using either the serial or parallelized version of the BSR code [12]. The distinctive feature of the method is the use of B-splines as a universal basis to represent the scattering orbitals in the inner region of $r \leqslant a$. Hence, the

R-matrix expansion in this region takes the form

$$\Psi_k(x_1,\ldots,x_{N+1}) = \mathcal{A}\sum_{ij}\bar{\Phi}_i(x_1,\ldots,x_N;\hat{\mathbf{r}}_{N+1}\sigma_{N+1})\,r_{N+1}^{-1}\,B_j(r_{N+1})a_{ijk} + \sum_i \chi_i(x_1,\ldots,x_{N+1})\,b_{ik}. \quad (2)$$

Here the $\bar{\Phi}_i$ denote the channel functions constructed from the N-electron target states, while the splines $B_j(r)$ represent the continuum orbitals. The χ_i are additional $(N+1)$-electron bound states. In standard R-matrix calculations [20], the latter are included one configuration at a time to ensure completeness of the total trial wave function and to compensate for orthogonality constraints imposed on the continuum orbitals. The use of nonorthogonal one-electron radial functions in the BSR method, on the other hand, allows us to completely avoid these configurations for compensating orthogonality restrictions. This procedure has practical advantages in reducing the pseudoresonance structure in the scattering solutions (see, for example, the discussion in Ref. [21]). Usually, the bound channels in the BSR calculations are employed for a more accurate description of the true bound states in the collision system.

In the present calculations, the bound channels were only used for an accurate description of the $(3s^23p^2)\,^3P$, ^1D, and ^1S negative-ion states. These states are located very close to the ground state, and hence their position is very sensitive to the balance of correlation corrections in the N-electron target and the $(N+1)$-electron scattering functions. To maintain this balance, the multiconfiguration expansions for the $3s^23p^2$ states were obtained in the same approximation as for the aluminum target states. We included all single and double excitations from the $3s$ and $3p$ orbitals to the $4l$ correlated orbitals. Our affinities of -0.404 and -0.093 eV for the $(3s^23p^2)\,^3P$ and ^1D states agree well with the experimental values of -0.433 and -0.095 eV, respectively [22]. The $(3s^23p^2)\,^1S$ state is a negative-ion resonance. According to our calculations, it lies 0.333 eV above the Al ground state.

The B-spline basis in the present calculations with the $r = 50a_0$ $(30a_0)$ box contained 111 (77) splines of order 8. The maximum interval in both grids was $0.65a_0$, which is sufficient for a good representation of the scattering electron wave functions for energies up to 150 eV. The BSR-587 collision model contained up to 1515 scattering channels, leading to generalized eigenvalue problems with matrix dimensions up to 100 000 in the B-spline basis. Direct numerical calculations were performed for partial waves with total orbital angular momentum $L \leqslant 25$. Taking into account the total spin and parity resulted in 104 partial waves overall. The calculation for the external region was performed with a parallelized version of the STGF program [23] whose top-up procedures were used to estimate the contribution from higher L values if needed.

III. RESULTS

The elastic cross sections shown in Fig. 1 exhibit a complicated energy dependence due to various partial-wave and resonance contributions. In particular, the shoulder at low energies is due to the $(3s^23p^2)\,^1S$ resonance, whereas

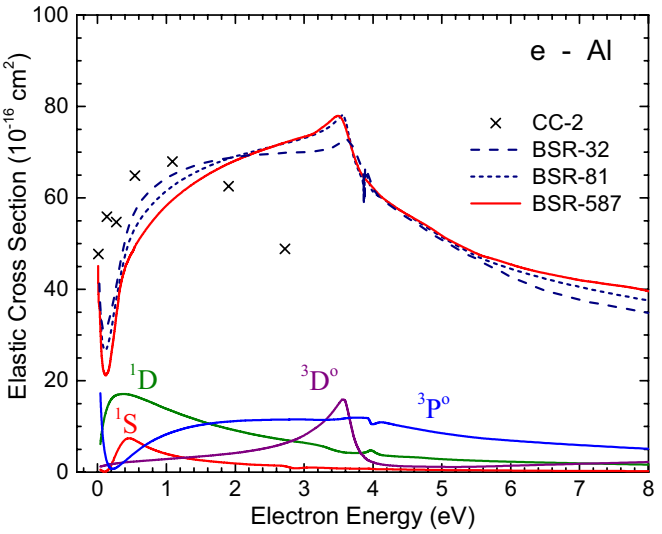

FIG. 1. (Color online) Cross sections for elastic electron scattering from aluminum atoms in their $(3s^23p)^2P^o$ ground state. The current BSR-32, BSR-81, and BSR-587 results are compared with those from two-state close-coupling calculations (CC-2) by Ryabikh and Fabricant [7]. Also shown are the contributions from the dominant partial waves.

the sharp peak at 3.7 eV is caused by the $(3s3p^3)\,^3D^o$ resonance. The elastic cross section near threshold is mainly defined by the $(3s^23p\,ks)\,^3P^o$ channel, with a predicted scattering length of $-2.33a_0$. This partial wave also exhibits a Ramsauer minimum. Comparison of results from different models reveals a slow convergence for the elastic cross section at low energies. Including the continuum pseudostates in the BSR-587 model leads to changes up to 10% in comparison to the BSR-81 predictions. This outcome is partly related to the extent to which the polarization of the target charge cloud by the scattering electron is included. The BSR-587 expansion yields the ground-state polarizability as $58.5a_0^3$, in good agreement with other available calculations [24] that predict the polarizability in the range of $55a_0^3$–$60a_0^3$. The two-state results of Ryabikh and Fabricant [7] agree rather well with the present cross sections up to 2 eV, but then differ in the energy dependence at higher incident energies.

Cross sections as a function of energy for the most important transitions from the ground state and between the excited states are presented in Figs. 2–4 for dipole-allowed, nondipole, and exchange transitions, respectively. Due to the almost complete absence of other theoretical results and experimental data, we compare our predictions from different models, which differ by the continuum pseudostates included. This allows us to check the convergence of the close-coupling expansion.

As seen from Fig. 2, adding more channel coupling results in a significant reduction of the predicted cross sections at low and intermediate electron energies. This holds for coupling to both the bound states and the continuum pseudostates. Coupling to the bound states is illustrated by comparing the BSR-10 and BSR-02 predictions, with the latter being close to the distorted-wave approximation. The coupling considerably reduces the theoretical cross sections at near-threshold energies. Inclusion of the $3s3p^2$ autoionizing states and a

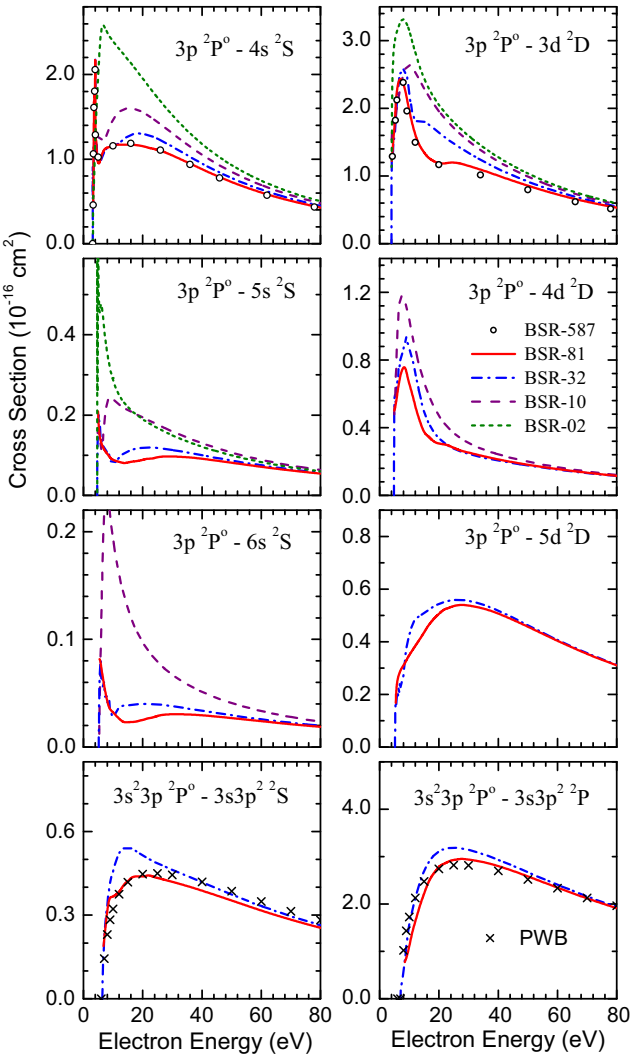

FIG. 2. (Color online) Cross sections as a function of collision energy for selected dipole-allowed transitions in aluminum. The current BSR results from different approximations are compared to illustrate the convergence of the close-coupling expansion. Also shown are the f-scaled plane-wave Born calculations (PWB) of Kim and Stone [8] for excitation of the $(3s3p^2)\,^2S$ and ^2P states.

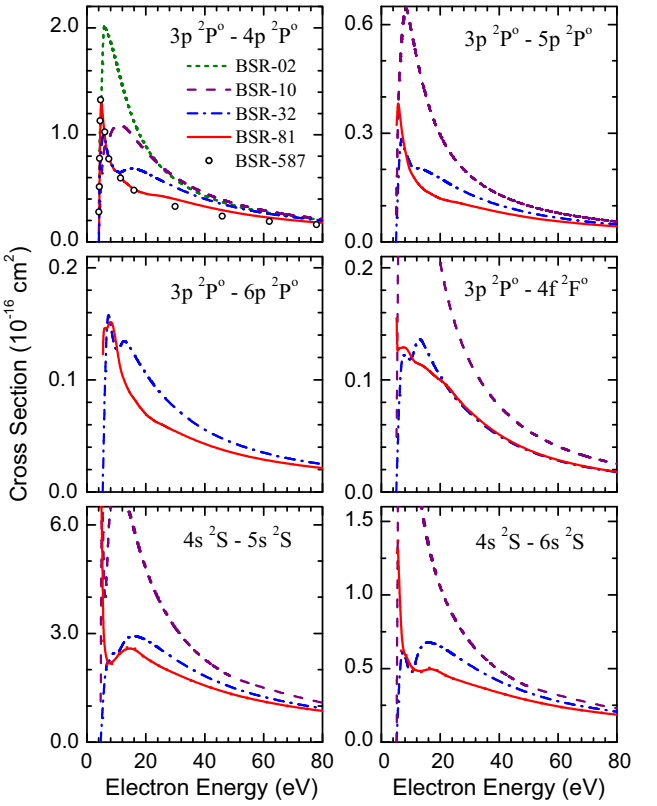

FIG. 3. (Color online) Cross sections as a function of collision energy for the most important nondipole transitions in aluminum. The current BSR results from different approximations are compared to illustrate the convergence of the close-coupling expansion.

few low-lying continuum pseudostates in the BSR-32 model further reduces the cross-section maximum, but the details strongly depend on the transition under consideration. A more pronounced effect was found for the $3p$-ns transitions than for the $3p$-nd transitions. The inclusion of additional pseudostates in the BSR-81 model further reduces the cross sections at intermediate energies, but the reduction is diminishing. As shown by the $3p$-$4s$ and $3p$-$3d$ excitations, inclusion of further pseudostates in the BSR-587 model does not change the resulting cross sections noticeably. Consequently, we consider the BSR-81 results converged at the few-percent level. Figure 2 also shows the important excitations of the $(3s3p^2)\,^2P$ and ^2S auto-ionizing states. These are strong transitions that considerably contribute to ionization (see below). The present BSR predictions closely agree with the plane-wave Born (PWB) cross sections [8], after scaling the latter by experimental oscillator strengths and shifting the maximum by an empirical procedure described in [25].

A strong influence of channel coupling is also found for nondipole transitions presented in Fig. 3. Here large corrections due to close-coupling effects are seen for transitions from the ground state as well as for transitions between excited states. Some of these transitions are relatively strong, comparable in magnitude to dipole-allowed excitations. Comparison of the BSR-10, BSR-32, and BSR-81 results shows that coupling to the bound states is dominant and hence the influence of the continuum pseudostates is relatively small. This suggests that the nondipole transitions may have large contributions from two virtual dipole transitions through an intermediate state. For the $3p$-$4p$ excitation, the BSR-81 and BSR-587 results are very close to each other, once again suggesting essential convergence of the predicted cross sections.

The exchange transitions shown in Fig. 4 are all connected with the $(3s3p^2)\,^4P$ metastable state. All exchange cross sections exhibit a strong low-energy maximum and quickly fall off with increasing incident electron energy. Coupling effects are much less pronounced here, with a larger influence due to bound-state coupling than to the influence of the continuum pseudostates.

Results for the ionization cross sections are presented in Fig. 5. The BSR-587 results were obtained as the sum of the excitation cross sections to all aluminum autoionizing states and the continuum pseudostates. We assumed that the radiative

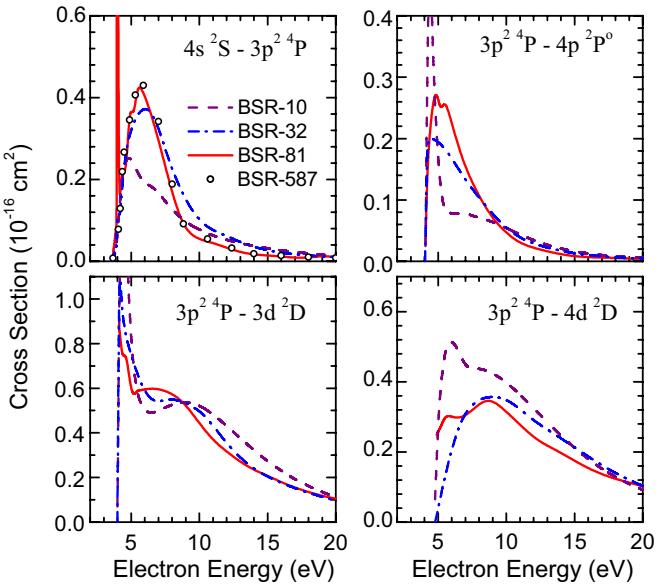

FIG. 4. (Color online) Cross sections as a function of collision energy for the most important exchange transitions in aluminum. The current BSR results from different approximations are compared to illustrate the convergence of the close-coupling expansion.

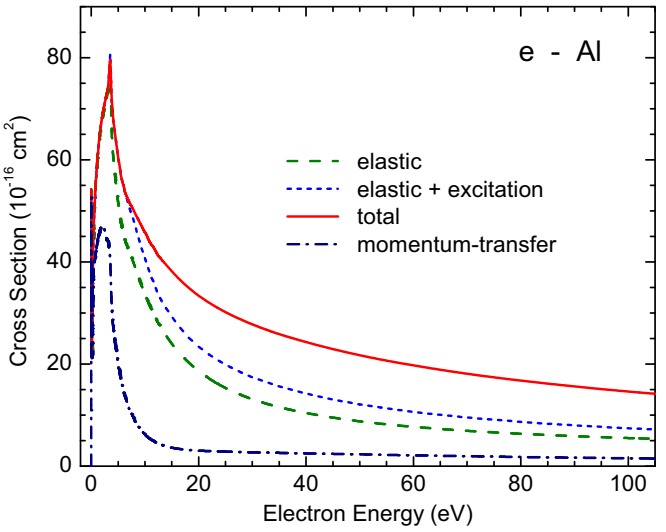

FIG. 6. (Color online) Grand total cross section for electron collisions with aluminum atoms in their $(3s^2 3p)\,^2P^o$ ground state, along with the contributions from elastic scattering alone and elastic scattering plus excitation processes, as well as the momentum-transfer cross section.

decay of the autoionizing states is negligible in comparison to the autoionization channel, except for the $(3s3p^2)\,^2P$ state. Here we used the autoionizing branching ratio of 0.9, in accordance with the autoionizing width calculations of [8]. The present BSR-587 results agree closely with the experimental data [6] for all electron energies. The RMPS cross sections [9] are given only for low energies up to 30 eV. They exceed the present results by 10–15%. The TDCC results [9], on the other hand, lie far below the BSR and RMPS predictions. Figure 5 also presents the direct ionization cross section. The deviation from the total ionization cross section suggests substantial excitation-autoionization contributions, which mainly originate from strong inner-subshell $3s$-$3p$ excitation to the $(3s3p^2)\,^2P$ and ^2S states. Note that the TDCC model did not include these important excitation-autoionization contributions, and hence its predictions are too small. Close agreement is also found with the BEB results [8]. As mentioned above, this is partly explained by the present cross sections for excitation of the $(3s3p^2)$ states being in close agreement with the scaled PWB results used in the BEB calculations.

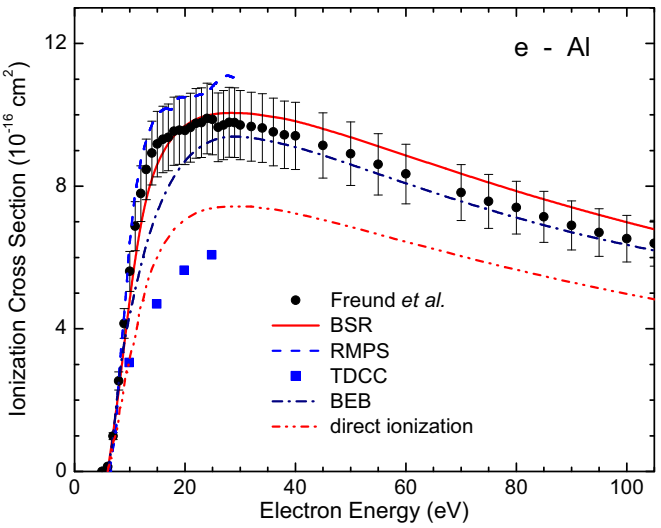

FIG. 5. (Color online) Cross sections for electron-impact ionization of aluminum from the $(3s^2 3p)\,^2P^o$ ground state. The present BSR results are compared with those from RMPS and TDCC [9] calculations, with the BEB results [8], and with the experimental data of Freund *et al.* [6]. Also shown is the direct ionization cross section.

Finally, Fig. 6 exhibits the grand total cross section for electron collisions with aluminum atoms in their $3s^2 3p$ ground state, i.e., the sum of angle-integrated elastic, excitation, and ionization cross sections. While the elastic cross section provides the largest contribution at low and intermediate energies, ionization dominates at 30 eV and above. Overall, the excitation processes represent less than 10% of the grand total cross section. Since the momentum transfer rather than the elastic cross section is typically important for plasma modeling, it is also shown in Fig. 6. The difference between the elastic and the momentum-transfer cross sections is substantial over the entire energy range. Hence, simply using the elastic cross section is not recommended as a substitute when the momentum-transfer result is not available.

IV. SUMMARY

We have presented an extensive set of electron scattering data for neutral aluminum, including elastic scattering, momentum transfer, excitation processes, and ionization of the ground state. State-to-state excitation cross sections were obtained for all transitions between 14 states of aluminum, and results were presented and discussed for selected transitions. The calculations were performed with the BSR code [12], in

which a *B*-spline basis is employed to represent the continuum functions inside the *R*-matrix sphere. The distinguishing feature of the BSR calculations is the use of nonorthogonal orbitals, both in constructing the target wave functions and in representing the scattering functions. This technique allows us to generate an accurate target description and to minimize pseudoresonance structure at higher energies. In particular, we accurately represented the strong interaction of the $(3s3p^2)\,^2D$ state with the $3s^2nd$ Rydberg series, which is a distinguished feature of the Al spectrum.

Given the lack of available experimental and theoretical data, it is crucial that theoretical predictions are validated in some way. Our most extensive calculations included 587 states. To check such important effects as target polarization and excitation to the target continuum, we compared the results with less extended models that only included bound and autoionizing states. The influence of the target continuum was found to be significantly less than seen before for atoms with a partially filled $2p$ shell such as C [26], N [27], and F [28]. The close agreement between our BSR-81 and BSR-587 predictions suggests that the present cross sections can be considered as converged to an accuracy of a few percent.

The elastic cross section at low energies exhibits several distinctive resonance features. Convergence of the close-coupling expansion in this case is slower than for the excitation cross sections. The momentum-transfer cross section, which is generally used in plasma modeling, differs significantly from the elastic cross section. We also obtained close agreement with experiment for the ionization cross section. This ensures us that the pseudostate close-coupling approach is, once again, working very well. Electronic files with the present results, for electron energies up to 100 eV, are available from the authors upon request.

ACKNOWLEDGMENTS

The large calculations were carried out on the Stampede supercomputer at the Texas Advanced Computing Center and on Gordon at the San Diego Supercomputer Center. This work was supported by the U.S. National Science Foundation under Grants No. PHY-1212450, No. PHY-1403245, and No. PHY-1520970, and by the XSEDE supercomputer allocation PHY-090031.

[1] Z. Chaoui and N. Bouarissa, Phys. Lett. A **297**, 432 (2002).
[2] H. Deutsch, K. Hilpert, K. Becker, M. Probst, and T. D. Märk, J. Appl. Phys. **89**, 1915 (2001).
[3] R. Dexter, D. Kerst, T. Lovell, S. Prager, and J. Sprott, Fusion Technol. **19**, 131 (1991).
[4] S. Kumar, D. Den Hartog, R. Magee, G. Fiksel, and D. Craig, Plasma Phys. Control. Fusion **53**, 032001 (2011).
[5] L. L. Shimon, E. I. Nepiypov, and I. P. Zapesochnij, Ukr. J. Phys. **20**, 229 (1975).
[6] R. S. Freund, R. C. Wetzel, R. J. Shul, and T. R. Hayes, Phys. Rev. A **41**, 3575 (1990).
[7] Ya. Ryabikh and I. Fabricant, J. Phys. B **14**, 349 (1981).
[8] Y.-K. Kim and P. M. Stone, Phys. Rev. A **64**, 052707 (2001).
[9] S. D. Loch, C. P. Ballance, D. Wu, Sh. A. Abdel-Naby, and M. S. Pindzola, J. Phys. B **45**, 065201 (2012).
[10] The Editors, Phys. Rev. A **83**, 040001 (2011).
[11] H. Chung, K. Bartschat, J. Tennyson, and D. R. Schultz, *Uncertainty Assessment for Theoretical Atomic and Molecular Scattering Data*, INDC(NDS)-0669 report (Vienna, Austria, 2014).
[12] O. Zatsarinny, Comp. Phys. Commun. **174**, 273 (2006).
[13] O. Zatsarinny and K. Bartschat, Phys. Rev. A **77**, 062701 (2008).
[14] O. Zatsarinny and K. Bartschat, J. Phys. B **46**, 112001 (2013).
[15] O. Zatsarinny and C. Froese Fischer, Comput. Phys. Commun. **180**, 2041 (2009).
[16] A. W. Weiss, Phys. Rev. A **9**, 1524 (1974).
[17] C. Froese Fischer, Comp. Phys. Commun. **176**, 559 (2007).
[18] I. Bray, K. Bartschat, and A. T. Stelbovics, Phys. Rev. A **67**, 060704(R) (2003).
[19] http://physics.nist.gov/cgi-bin/AtData.
[20] P. G. Burke, *R-Matrix Theory of Atomic Collisions* (Springer-Verlag, Berlin, 2011).
[21] S. S. Tayal and O. Zatsarinny, Phys. Rev. A **78**, 012713 (2008).
[22] M. Scheer, R. C. Bilodeau, J. Thøgersen, and H. K. Haugen, Phys. Rev. A **57**, R1493(R) (1998).
[23] N. Badnell, J. Phys. B **32**, 5583 (1999); see also http://amdpp.phys.strath.ac.uk/UK_RmaX/codes.html.
[24] http://ctcp.massey.ac.nz/dipole-polarizabilities.
[25] Y.-K. Kim, Phys. Rev. A **64**, 032713 (2001).
[26] Y. Wang, O. Zatsarinny, and K. Bartschat, Phys. Rev. A **87**, 012704 (2013).
[27] Y. Wang, O. Zatsarinny, and K. Bartschat, Phys. Rev. A **89**, 062714 (2014).
[28] V. Gedeon, S. Gedeon, V. Lazur, E. Nagy, O. Zatsarinny, and K. Bartschat, Phys. Rev. A **89**, 052713 (2014).